good approximation for **1** (Table I). As a consequence, the estimate of the effect of quadruple excitations (Davidson's correction) does not heavily modify the energy difference (Table VII). For system **4**, the weight of the reference configurations is significantly higher for the singlet than for the triplet state (Table I) and Davidson's correction strongly reduces the S-T difference from 2380 to 680 cm^{-1}. A more extended CI calculation or a perturbative estimate should be necessary to refine this latter value.

The S-T separation for **1** has been estimated from NMR spectroscopy as 22-24 kJ mol^{-1},[8] that is, 1840-2000 cm^{-1}, in reasonably good agreement with the value computed in the present work (2820 cm^{-1}).

Conclusion

Four binuclear complexes of vanadium assumed from electron counting considerations to exhibit strikingly different electronic structures affecting the dimetal unit have been investigated by means of a multistep ab initio CI treatment. It appears from the calculations that in spite of different V-V bond orders, varying from 1 to 3, the four complexes share several characters and properties, such as a slightly negative net charge for the metal atoms, a computed bond order between 1.15 and 1.50, and the presence of a low-lying triplet state at less than 3000 cm^{-1} above the singlet ground state. These computed similarities should be compared to the relatively short range of the V-V distanced between 2.315 and 2.439 Å. The calculations show that two types of contributions to the metal-metal interaction should be considered. On the one hand, weak, direct interactions of the δ and σ types are responsible for the small singlet-triplet energy gap. Due to an important relocalization effect evidenced from the natural orbital occupation numbers, those interactions give little contribution to the computed bond order. On the other hand, delocalized metal-ligand-metal interactions with V-V bonding character are present in all four complexes. These interactions may either correspond to formal metal-metal bonds as in **1** and **3** or result from the stabilization of ligand orbitals by V-V bonding orbital combinations as in **2** and **4**. The resulting orbitals are little affected by correlation effects, and the metal contribution therefore remains bonding and delocalized. These MOs provide an important contribution to the computed V-V bond order. The electronic structure of the dimetal subunit that can be formally deduced from electron counting considerations is therefore subject to important corrections in opposite directions. On the one hand, relocalization of through-space metal-metal bonding electrons considerably reduces their contribution to the bond order. On the other hand, delocalized electrons that should be in most cases formally attributed to the ligands do provide the largest share of the metal-metal bonding. Relocalization prevails for complexes with formal multiple V-V bonds (**1**, **2**, and **3**), and the formal bond order is reduced by a factor close to 2. In contrast, delocalized bonding raises the bond order of **4** from 1, the formal value in the leading configuration, to 1.45. The result is an equalization of the electronic properties of the four complexes and a greater sensitivity of the structural parameters to the metal-ligand rather than to the metal-metal interaction.

Acknowledgment. We are pleased to thank Pr. C. Krüger and Dr. R. Goddard for a stimulating discussion. All calculations have been carried out on the CRAY-2 computer at the CCVR (Palaiseau, France) through a grant of computer time from the Conseil Scientifique du Centre de Calcul Vectoriel de la Recherche.

Registry No. **1**, 107201-40-1; **2**, 104462-69-3; **3**, 104598-74-5; **4**, 86421-59-2.

Electron Propagator Theory of the Ground and Excited States of $CaBH_4$

J. V. Ortiz

Contribution from the Department of Chemistry, University of New Mexico, Albuquerque, New Mexico 87131. *Received August 13, 1990*

Abstract: Electron propagator theory provides a correlated one-electron picture of bonding in various states of $CaBH_4$. Calculations of $CaBH_4^+$ electron affinities produce ground- and excited-state energies at the optimized, C_{3v} minimum of the neutral ground state and at a C_{2v} geometry. Contour plots and expectation values of Feynman-Dyson amplitudes (FDA's) describe the distribution of the least bound electron in various states. $\tilde{X}^2A_1$ has an unpaired electron in a Ca sp hybrid polarized away from BH_4. Splittings of Ca d orbitals, variable hybridization with Ca p orbitals, and contrasting Ca-ligand bonding properties characterize the next few states, which display π, σ, and δ pseudosymmetry in their FDA's. The splitting of the first two excited states is not as large as it is in calculations where BH_4 is replaced by a ligand which confronts Ca with a lone pair of electrons with σ pseudosymmetry. Higher excited states have electrons in diffuse orbitals that have been orthogonalized to the bonding regions.

I. Introduction

Many radicals composed of Ca and a ligand with a positive electron affinity have a single electron localized about Ca. Several spectroscopic investigations of $C_{\infty v}$ examples have confirmed this simple picture, where several orbitals with σ, π, or δ symmetry, often exhibiting considerable mixing among metal s, p, and d orbitals, can accept the least bound electron.[1-3] When the ligand is not linear, for example, NH_2 or CH_3, cylindrical pseudosymmetry, defined by an axis connecting Ca to the other non-hydrogen nucleus, remains useful as an organizing principle.[4] Even for a linear ligand entering into a nonlinear arrangement with Ca, as in CaSH, this scheme retains its qualitative validity.[5] $CaBH_4$ is unlike previously studied molecules in that the ligand does not present the metal with a single lone pair of electrons with σ pseudosymmetry. Borohydride anion generally binds to metal

(1) Nakagawa, J.; Domaille, P. J.; Steimle, T. C.; Harris, D. O. *J. Mol. Spectrosc.* **1978**, *70*, 374. Dulick, M.; Bernath, P. F.; Field, R. W. *Can J. Phys.* **1980**, *58*, 703. Bernath, P. F.; Field, R. W. *J. Mol. Spectrosc.* **1980**, *82*, 339.

(2) Wormsbecher, R. F.; Trkula, M.; Martner, C.; Penn, R. E.; Harris, D. O. *J. Mol. Spectrosc.* **1983**, *97*, 29. Hilborn, R. C.; Qingshi, Z.; Harris, D. O. *J. Mol. Spectrosc.* **1983**, *97*, 73. Bernath, P.; Kinsey-Nielsen, S. *Chem. Phys. Lett.* **1984**, *105*, 663. Bernath, P. F.; Brazier, C. R. *Astrophys. J.* **1985**, *288*, 373.

(3) Ellingboe, L. C.; Bopegedera, A. M. R. P.; Brazier, C. R.; Bernath, P. F. *Chem. Phys. Lett.* **1986**, *126*, 285. Bopegedera, A. M. R. P.; Brazier, C. R.; Bernath, P. F. *Chem. Phys. Lett.* **1987**, *136*, 97. Bopegedera, A. M. R. P.; Brazier, C. R.; Bernath, P. F. *J. Mol. Spectrosc.* **1988**, *129*, 268. Brazier, C. R.; Bernath, P. F. *J. Chem. Phys.* **1988**, *88*, 2112.

(4) Ortiz, J. V. *J. Chem. Phys.* **1990**, *92*, 6728.

(5) Ortiz, J. V. *Chem. Phys. Lett.* **1990**, *169*, 116.

0002-7863/91/1513-1102$02.50/0

cations through two or three hydrogen bridges, creating a coordination environment in which Ca is confronted by an occupied σ and either one (bidentate case) or two (tridentate case) occupied π ligand orbitals. Each orbital belongs to the t_2 set of highest occupied molecular orbitals of BH_4^- and consists of a bonding combination of B p orbitals and H s orbitals. On the basis of simple notions of overlap and energy matching, one would expect states with a Ca-centered electron in a σ pseudosymmetry level to be stabilized, while the π pseudosymmetry levels are destabilized, in comparison with other molecules.

Electron propagator[6] programs calculate electron affinities of $CaBH_4^+$ at the neutral's geometry and yield excitation energies. Feynman–Dyson amplitudes (FDA's) accompanying the electron affinities provide information on how the electronic structure of each neutral state differs from that of the cation. Electron propagator theory produces electron binding energies and FDA's that reflect the effects of electron correlation, thus providing a one-electron picture of bonding that is as easily interpretable as molecular orbital theory.

II. Methods

Standard programs[7] optimize equilibrium geometries of the neutral. Second-order many-body perturbation theory, also known as MP2, incorporates the major effects of electron correlation, where the reference state is the unrestricted Hartree–Fock wave function.[8-10] The configuration of this different-orbitals-for-different-spins, reference state wave function has nine a_1 and six e α spin orbitals and eight a_1 and six e β spin orbitals. Geometry optimization on $\tilde{X}^2A_1$ employs 6-31+G(d,p)[11] B and H and (43321/431/51) Ca basis sets[4,5]. The latter decontracts the three primitive Gaussian expansions of the 4s Ca atomic orbital and includes a set of p polarization functions.[12] An uncontracted Ca d function in terms of six primitive Gaussians derives from atomic calculations on the ^3D state.[13] Calculations of this type yield bond lengths approximately 0.04 Å longer than experiment.[2,4,5]

An electron propagator program[14,15] (EPT90) compatible with Gaussian 88[7] calculates vertical electron affinities of the cations.[16] The Møller–Plesset partitioning of the Hamiltonian[8] defines finite order relaxation and correlation corrections to Koopmans's theorem.[17] Electron propagator calculations determine electron binding energies and FDA's without final state wave functions. The FDA's are defined by

$$\int \Psi^*_N(x_2,x_3,x_4,...,x_{N+1})\Psi_{N+1}(x_1,x_2,x_3,...,x_{N+1})\,dx_2\,dx_3\,dx_4...dx_{N+1} = \phi^{FDA}(x_1)$$

and

$$\int \Psi^*_{N-1}(x_2,x_3,x_4,...,x_N)\Psi_N(x_1,x_2,x_3,...,x_N)\,dx_2\,dx_3\,dx_4...dx_N = \phi^{FDA}(x_1)$$

Table I. Optimized Geometries

Parameter	C_{3v} Hartree–Fock	C_{3v} correlated	C_{2v} Hartree–Fock	C_{2v} correlated
Ca–B, Å	2.485	2.430	2.691	2.606
B–H_t, Å	1.192	1.188	1.205	1.200
B–H_b, Å	1.248	1.234	1.266	1.242
Ca–B–H_t, deg	180	180	122.1	122.2
Ca–B–H_b, deg	67.3	67.3	53.6	54.4

Table II. C_{3v} Harmonic Frequencies (cm^{-1})

symmetry	freq	symmetry	freq
A_1	479	A_1	1290
E	528	E	2354
E	1175	A_1	2363
E	1284	A_1	2716

for electron affinities and ionization energies, respectively. EPT90 obtains poles and residues of the Dyson equation

$$\mathbf{G}^{-1}(E) = \mathbf{G}_0^{-1}(E) - \mathbf{\Sigma}(E)$$

Poles, values of E such that the determinant of $\mathbf{G}^{-1}(E)$ is zero, equal electron binding energies. Poles of the unperturbed propagator matrix, $\mathbf{G}_0(E)$, where

$$\{\mathbf{G}_0^{-1}(E)\}_{ij} = (E - \epsilon_i)_{ij}$$

and ϵ_i is the ith canonical orbital energy, produce Koopmans's theorem[17] results. Relaxation and correlation effects reside in the self-energy matrix, $\mathbf{\Sigma}(E)$.

Electron affinities of the cation are calculated at the optimized geometry of the neutral. Differences between these electron affinities provide excitation energies. Some electron propagator calculations neglect nondiagonal elements of the self-energy matrix. Because $G_0^{-1}(E)$ is already diagonal, these calculations require the calculation of diagonal elements only of $\mathbf{G}^{-1}(E)$. Setting these elements to zero implies that one must search for values of E such that

$$E = \epsilon_i + \Sigma(E)_{ii}$$

This approximation forces the FDA to be a canonical molecular orbital. Programs perform second-order, third-order, and partial fourth-order self-energy[15,18] iterations, omitting only core orbitals from diagram summations. In addition, nondiagonal second-order calculations have been carried out in order to check the validity of the diagonal approximation. For nondiagonal calculations, one must diagonalize

$$\epsilon + \mathbf{\Sigma}(E)$$

for various values of E with the goal of finding an eigenvalue equal to E. The eigenvector fulfilling this condition provides the linear combination of canonical orbitals that equals the FDA.

Propagator calculations require diffuse Ca functions to describe neutral excited states. 1,1,1 decontraction of the 4s Ca atomic orbital, adoption of a double p polarization set,[12] and addition of diffuse s (exponents: 0.0075, 0.00225), p (exponent: 0.0069), and d (exponents: 0.0125, 0.00375) functions fulfill this need. Calculations with the resulting (8s,5p,4d) Ca and 6-31+G(d,p) ligand basis sets render neutral excitation energies within 0.1 eV of experiment for $CaCH_3$, $CaNH_2$, CaOH, CaF, and CaSH.[4,5]

Additional diffuse exponents are devised by multiplying the exponent of the most diffuse basis function of the previous basis with the same angular dependence by a factor of 0.3. Extra functions on Ca or on the ligand nuclei have been generated in this way.

Plots of the FDA's are drawn in order to interpret the data. Contours in intervals of 0.015 are shown in the figures. Solid (dotted) contours represent positive (negative) values while dashed contours denote nodes. FDA's are equivalent to canonical molecular orbitals when the diagonal self-energy approximation is made. For nondiagonal calculations, FDA's reflect relaxation and correlation effects.

Expectation values of the FDA's

$$\int \phi^{FDA*}(1)\hat{O}(1)\phi^{FDA}(1)\,d(1) = \langle\hat{O}\rangle$$

provide measures of distributions and bonding properties. For calculations in which diffuse electronic distributions are important, procedures that assign charges to basis orbitals may produce erratic trends. Eval-

(6) Linderberg, J.; Öhrn, Y. *Propagators in Quantum Chemistry*; Academic Press: New York, 1973. von Niessen, W.; Schirmer, J.; Cederbaum, L. S. *Comput. Phys. Rep.* **1984**, *1*, 57. Herman, M. F.; Freed, K. F.; Yeager, D. L. *Adv. Chem. Phys.* **1981**, *48*, 1. Öhrn, Y.; Born, G. *Adv. Quantum Chem.* **1981**, *13*, 1. Simons, J. In *Theoretical Chemistry: Advances and Perspectives*; Eyring, H., Ed.; Academic Press: New York, 1978.

(7) Gaussian 88: Frisch, M. J.; Head-Gordon, M.; Schlegel, H. B.; Ragavachari, K.; Binkley, J. S.; Gonzalez, C.; DeFrees, D. J.; Fox, D. J.; Whiteside, R. A.; Seeger, R.; Melius, C. F.; Baker, J.; Martin, R.; Kahn, L. R.; Stewart, J. J. P.; Fluder, E. M.; Topiol, S.; Pople, J. A. Gaussian, Inc.: Pittsburgh, PA, 1988.

(8) Møller, C.; Plesset, M. S. *Phys. Rev.* **1934**, *46*, 618.

(9) Binkley, J. S.; Pople, J. A. *Int. J. Quantum Chem.* **1975**, *9*, 229.

(10) Bartlett, R. J. *Annu. Rev. Phys. Chem.* **1981**, *32*, 359.

(11) Hehre, W. J.; Ditchfield, R.; Pople, J. A. *J. Chem. Phys.* **1972**, *56*, 2257. Clark, T.; Chandrasekhar, J.; Spitznagel, G. W.; Schleyer, P. v. R. *J. Comput. Chem.* **1983**, *4*, 294. Hariharan, P. C.; Pople, J. A. *Theor. Chim. Acta* **1973**, *28*, 213.

(12) *Gaussian Basis Sets For Molecular Calculations*; Huzinaga, S., Ed.; Elsevier: Amsterdam, 1984.

(13) Hay, P. J. Private communication.

(14) Ortiz, J. V. *Int. J. Quantum Chem., Quant. Chem. Symp.* **1987**, *21*, 469.

(15) Ortiz, J. V. *Int. J. Quantum Chem., Quant. Chem. Symp.* **1988**, *22*, 431.

(16) EPT90, an electron propagator program by J. V. Ortiz, University of New Mexico, 1990.

(17) Koopmans, T. C. *Physica* **1933**, *1*, 104.

(18) Ortiz, J. V. *J. Chem. Phys.* **1988**, *89*, 6348.

Table III. C_{3v} Electron Affinities (eV)

final state	Koopmans's theorem	diagonal 2nd	nondiagonal 2nd	diagonal 3rd	diagonal partial 4th
$\tilde{X}^2A_1$	5.476	5.706	5.712	5.663	5.670
$\tilde{A}^2E$	3.613	3.808	3.818	3.776	3.783
$\tilde{B}^2A_1$	3.317	3.672	3.691	3.618	3.631
$\tilde{C}^2E$	2.678	3.071	3.099	3.008	3.023
$\tilde{D}^2A_1$	2.085	2.140	2.141	2.128	2.130
$\tilde{E}^2E$	1.636	1.768	1.844	1.747	1.752
$\tilde{F}^2A_1$	1.506	1.602	1.607	1.589	1.593
$\tilde{G}^2E$	1.361	1.446	1.460	1.447	1.451
$\tilde{H}^2E$	1.268	1.351	1.346	1.337	1.340

Table IV. C_{2v} Electron Affinities (eV)

final state	Koopmans's theorem	diagonal 2nd	diagonal 3rd	diagonal partial 4th
$\tilde{X}^2A_1$	5.461	5.858	5.829	5.837
$\tilde{A}^2B_1$	3.789	3.958	3.934	3.941
$\tilde{B}^2B_2$	3.736	3.932	3.915	3.925
$\tilde{C}^2A_1$	3.430	3.741	3.711	3.724
$\tilde{D}^2A_1$	2.875	3.255	3.215	3.232
$\tilde{E}^2A_2$	2.827	3.192	3.155	3.172
$\tilde{F}^2B_1$	2.317	2.734	2.702	2.720
$\tilde{G}^2A_1$	2.127	2.177	2.169	2.171
$\tilde{H}^2B_2$	1.707	1.876	1.858	1.865
$\tilde{I}^2A_1$	1.543	1.631	1.624	1.629
$\tilde{J}^2B_1$	1.585	1.623	1.619	1.621
$\tilde{K}^2B_2$	1.380	1.510	1.506	1.512
$\tilde{L}^2A_1$	1.319	1.393	1.384	1.388
$\tilde{M}^2A_2$	1.302	1.370	1.363	1.366

uation of FDA expectation values better serves the present explanatory goals.

III. Results

1. Structures. Two bridged structures, with C_{3v} and C_{2v} symmetry, are studied. The former has three symmetry equivalent hydrogen bridges between Ca and B, while the latter has just two symmetry equivalent hydrogen bridges. One terminal hydrogen is present in the C_{3v} structure, but there are two symmetry equivalent terminal hydrogens for the C_{2v} case. There is close agreement between the Hartree–Fock and correlated second-order geometries except for the distances between Ca and B. Structural parameters are shown in Table I. (H_b and H_t stand for bridge and terminal hydrogens, respectively.) Second-order total energies favor the triply bridged structure by 0.352 eV. Hartree–Fock total energies yield 0.291 eV for the same isomerization energy. Such close agreement leads one to expect that these predictions will not change much should higher order calculations be performed. Spin contamination in the unrestricted Hartree–Fock calculations is negligible: expectation values of S^2 differ from 0.75 by less than 0.01. Vibrational frequencies calculated at the correlated, triply bridged geometry are listed in Table II. The lowest frequency governs the Ca–BH_4 stretch and the next lowest frequency pertains to the lateral vibration of the borohydride ligand with respect to the Ca–B axis. Internal motions of the ligand atoms govern the other frequencies.

2. Ground- and Excited-State Energies. With use of the closed-shell cation as a reference state at the neutral's triply bridged geometry, EPT90 calculates electron affinities of the cation at various levels of theory that include corrections to Koopmans's theorem. These include nondiagonal second order and diagonal second, third, and partial fourth order. (See Table III.) The largest discrepancies are between the uncorrelated and diagonal second-order columns. Further refinements arising from inclusion of higher orders or from abandonment of the diagonal approximation are relatively small. Correlation corrections to Koopmans's theorem results tend to become smaller for the higher states.

Studies of the three lowest states are undertaken for augmented basis sets. Extra sets of s, p, and d diffuse functions on Ca with exponents of 0.000675, 0.00207, and 0.001125, respectively, are added and the diagonal calculations are redone. Discrepancies with Table III are 0.001 eV or less. These functions are discarded and extra diffuse functions on the ligand atoms are added. Hydrogen s functions with 0.0108 exponents and boron sp functions with 0.00945 exponents produce electron affinities within 0.02 eV of values in Table III. Previous studies[4,5] indicate that the present basis should yield electron binding energies that are stable with respect to basis set augmentations for the states presently under investigation.

Table V. Excitation Energies (eV)

C_{3v} final state	$CaBH_4$ excitation energy	C_{2v} final state	$CaBH_4$ excitation energy
$\tilde{X}^2A_1$	0	$\tilde{X}^2A_1$	0
$\tilde{A}^2E$	1.887	$\tilde{A}^2B_1$	1.896
		$\tilde{B}^2B_2$	1.912
$\tilde{B}^2A_1$	2.039	$\tilde{C}^2A_1$	2.113
$\tilde{C}^2E$	2.647	$\tilde{D}^2A_1$	2.605
		$\tilde{E}^2A_2$	2.665
$\tilde{D}^2A_1$	3.540	$\tilde{G}^2A_1$	3.666
$\tilde{E}^2E$	3.918	$\tilde{F}^2B_1$	3.117
		$\tilde{H}^2B_2$	3.972
$\tilde{F}^2A_1$	4.077	$\tilde{I}^2A_1$	4.208
$\tilde{G}^2E$	4.219	$\tilde{J}^2B_1$	4.216
		$\tilde{K}^2B_2$	4.325
$\tilde{H}^2E$	4.330	$\tilde{L}^2A_1$	4.449
		$\tilde{M}^2A_2$	4.471

Table VI. Nuclear Positions (au)

nucleus	x	y	z
Ca	0	0	1.409
B	0	0	−3.182
H_t	0	0	−5.427
H_b	0	2.151	−2.283

Diagonal calculations are performed at the optimum doubly bridged structure. These electron affinities are shown in Table IV. Convergence of results is similar to that obtained for the triply bridged structure.

Differences between the electron affinities provide vertical excitation energies of the neutral. Diagonal, partial fourth-order values are used to generate these predictions. Table V displays the correlation of levels between the two geometries. $\tilde{A}^2E$ of the tridentate structure splits into two levels, $\tilde{A}^2B_1$ and $\tilde{B}^2B_2$, separated by about 0.02 eV. In the first nondegenerate excited state, there is a slight destabilization, 0.07 eV, relative to the ground state in the bidentate geometry. In the $\tilde{C}^2E$ state, which contains an unpaired Ca d electron with Ca–B δ pseudosymmetry, a splitting into doubly bridged states with $^2A_1$ and $^2A_2$ symmetry takes place. For the next higher states, there are energy crossings between the two geometries. $\tilde{D}^2A_1$ of the triply bridged structure correlates with $\tilde{G}^2A_1$ of the doubly bridged structure, which is between two states that correlate with $\tilde{E}^2E$. The lower of these two states has undergone a considerable stabilization, from 3.918 to 3.117 eV, relative to the ground state in the bidentate geometry. However, most of the excitation energies increase in the C_{2v} structure.

3. C_{3v} Feynman–Dyson Amplitudes. Inspection of the second-order, nondiagonal FDA's for each cation electron affinity discloses how the neutral states are different from each other. For the present states, the canonical molecular orbitals corresponding to Koopmans's theorem are the dominant contributors to the nondiagonal, second-order FDA's. Pole strengths for each state are quite close to unity, indicative of the qualitative validity of the Koopmans description. Properties of the FDA's provide useful indices for comparison of spatial distributions and phase relationships.

For the ground state of the neutral in the triply bridged geometry, the FDA is primarily built from diffuse Ca s orbitals with a slight amount of p hybridization that distorts the s orbitals away from the ligand. Figure 1 shows this lobe, where the squares represent nuclear positions. (Ca is almost obliterated by the concentration of contours about its position on the z axis at z = 1.409.) Ca, B, H_t, and one of the symmetry equivalent H_b's lie in the plane (yz) of the graph. Positions of the nuclei in atomic

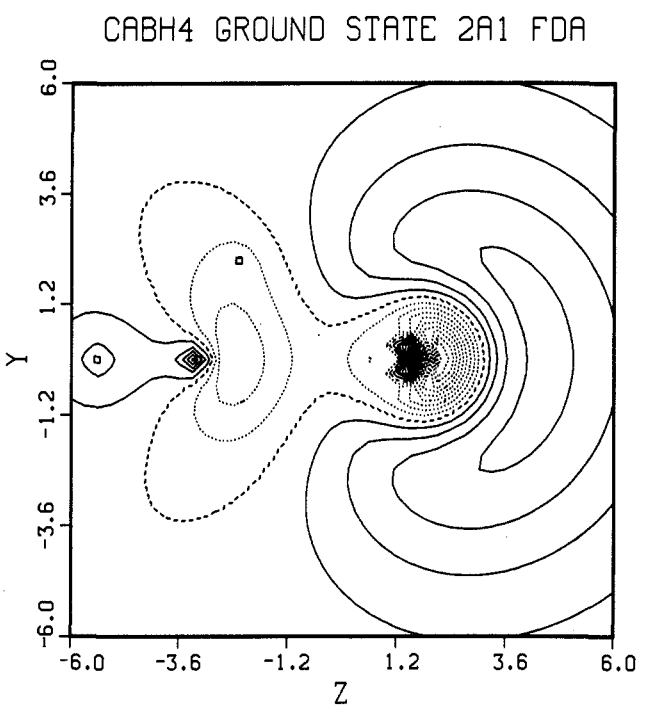

Figure 1. $\tilde{X}^2A_1$ Feynman–Dyson amplitude of C_{3v} $CaBH_4$.

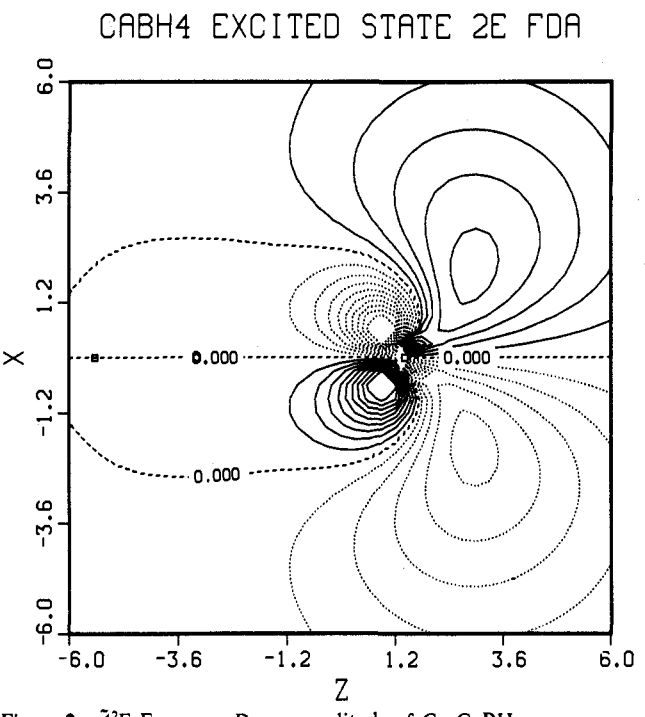

Figure 2. $\tilde{A}^2E$ Feynman–Dyson amplitude of C_{3v} $CaBH_4$.

Table VII. Expectation Values of FDA's (au)

property	$\tilde{X}^2A_1$	$\tilde{A}^2E$	$\tilde{B}^2A_1$	$\tilde{C}^2E$
kinetic energy	0.494	0.467	0.739	1.017
total nuclear attraction energy	−7.153	−6.730	−8.507	−10.015
$\langle z \rangle$	3.267	3.173	2.667	1.390
$\langle x^2 + y^2 \rangle$	13.354	22.335	11.742	15.126
Ca nuclear attraction energy	−5.807	−5.491	−6.972	−8.495
B nuclear attraction energy	−0.755	−0.687	−0.867	−0.925
H_t nuclear attraction energy	−0.116	−0.107	−0.125	−0.135
H_b nuclear attraction energy	−0.158	−0.146	−0.181	−0.200
E_z at Ca	0.041	0.007	−0.004	−0.001
E_z at B	0.019	0.017	0.028	0.028
E_z at H_t	0.012	0.011	0.015	0.017
E_z at H_b	0.019	0.017	0.026	0.030
E_y at H_b	−0.009	−0.007	−0.012	−0.012

units, determined by the correlated results of Table I, are given in Table VI. A nodal contour extends from an arc about the Ca to the bonding region between B and the bridge H's. One can understand this FDA as a Ca 4s–4p hybrid that has been orthogonalized to one of the borohydride's 3-fold degenerate highest occupied molecular orbitals.

A deeper insight into the nature of bonding in the neutral ground state is obtained through expectation values of the FDA. Table VII shows the FDA expectation values. The z component of position is polarized away from the ligand. Attraction to Ca is the largest part of the nuclear attraction energy. Division of the nuclear attraction energy components by the nuclear charges (20 for Ca, 5 for B, 1 for H) gives a rough measure of the electronic distribution. These values are approximately −0.29, −0.15, −0.12, and −0.16 for Ca, B, terminal H, and bridging H, respectively. It is clear that an electron in this FDA will sample the neighborhood around Ca more than that of any other nucleus. Electric fields are evaluated at the nuclear positions in order to obtain another measure of the FDA's distribution. z components are positive at each nucleus and the y component at the bridging H of Figure 1 is negative. When these values are weighted by the nuclear charges, the ligand nuclei will be drawn to the right, but the Ca will be drawn more. The net effect is what one might expect of an electron in a hybrid orbital that points away from the ligand: to draw the nearest nucleus away from its neighbors. If one eliminates the middle ground represented by the nonbonding classification, then this FDA must be categorized as Ca–ligand antibonding. One can expect that electron interaction will more fully screen attractions to the borohydride nuclei than the attraction to Ca.

$\tilde{A}^2E$ has an FDA dominated by Ca d and p orbitals with Ca–B π pseudosymmetry. Contours in the xz plane are displayed in Figure 2. Constructive interference of Ca p and d orbitals occurs away from the ligand. Contributions from basis orbitals on the ligand are negligibly small. The nodal surface extends over the entire BH_4 ligand. Expectation values of the FDA confirm the picture of a nonbonded hybrid of 4p and 3d Ca orbitals. Polarization along the z axis, as shown in the $\langle z \rangle$ value, is slightly less than that in the ground state. Nuclear attraction energies and forces on the nuclei are weaker than those in the ground state, especially for Ca. These trends imply that an electron in this FDA is more remote from all of the nuclei, but that the polarization away from the ligand takes place more in the x and y directions than in the z direction. The increase in $\langle x^2 + y^2 \rangle$ confirms this explanation.

$\tilde{B}^2A_1$'s FDA is composed chiefly of diffuse d orbitals on Ca and has small contributions from diffuse Ca p orbitals and the diffuse s orbital on B. Note the nodal surface that extends from the Ca nucleus and cuts through the B–H bond region close to the bridging H's. Another nodal surface encapsulates the B nucleus, indicative of 3s-like B contributions. Hydrogen participation is negligible. The value of $\langle z \rangle$ is considerably smaller, showing less polarization away from the ligand. Every nuclear attraction energy is more negative than in the ground state. Especially significant is the negative sign of the electric field at the Ca nucleus. All of the forces on the borohydride nuclei are greater than those in the ground state. These two contrasts imply that this FDA should be classified as more bonding (or less antibonding) between Ca and BH_4 than the other two FDA's. This is compatible with the gross features of Figure 3, which show constructive interference taking place in most of the Ca–H–B bridging region.

In order to put the bonding trends implied by the FDA analysis to an additional test, a new set of diagonal second-order calculations is performed without the most diffuse s, p, and d sets on Ca. At the same geometry, the electron affinities of the cation are virtually unchanged. Calculations are subsequently done at geometries that retain the internal structure of the borohydride ligand, but with different Ca–B distances in intervals of 0.05 Å. Combining the new electron affinities at each geometry with the second-order total energies of the cation reference state produces potential energy curves for each neutral state. An indication of

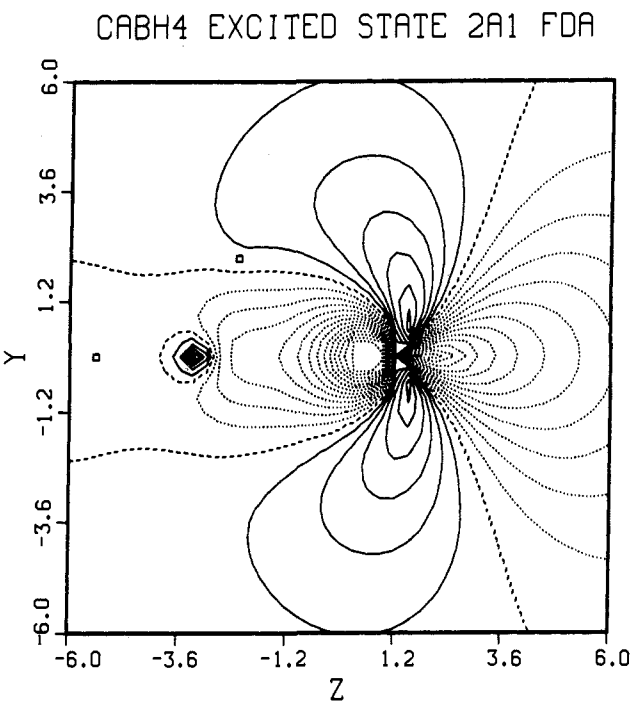

Figure 3. $\tilde{B}^2A_1$ Feynman–Dyson amplitude of C_{3v} $CaBH_4$.

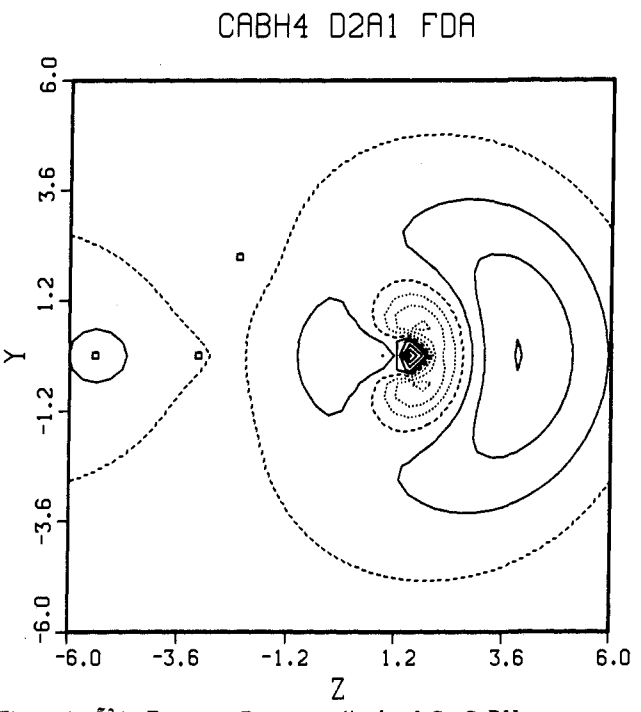

Figure 4. $\tilde{D}^2A_1$ Feynman–Dyson amplitude of C_{3v} $CaBH_4$.

Table VIII. Total Energies (au)

Ca–B, Å	$\tilde{X}^2A_1$	$\tilde{A}^2E$	$\tilde{B}^2A_1$
2.330	−703.21678	−703.14861	−703.14492
2.380	−703.21922	−703.15025	−703.14582
2.430	−703.22056	−703.15083	−703.14579
2.480	−703.22098	−703.15052	−703.14499
2.530	−703.22062	−703.14948	−703.14358

the weakness of the Ca–BH_4 stretching force constant is the flatness of the potential energy curves; total energies are listed in Table VIII. For the ground-state neutral, the minimum lies near 2.48 Å, while for the $\tilde{A}^2E$ and $\tilde{B}^2A_1$ states, the minima are near 2.43 and 2.38 Å, respectively. These results confirm the trends discussed above. The first excited state has an unpaired electron that is more nonbonding and less antibonding than its ground-state counterpart. A slight amount of Ca–ligand bonding character is introduced by the unpaired electron in the highest of the three states. That the minimum of the ground-state neutral does not coincide with that of the second-order many-body perturbation theory optimizations is another indication of the flatness of the potential energy surface with respect to Ca–B distance variations.

Analysis of the following state, $\tilde{C}^2E$, is relatively simple. Ca d orbitals with Ca–B δ pseudosymmetry are practically the sole contributors to the FDA. $\langle z \rangle$ is close to the position of the Ca nucleus. Translation of charge to smaller z is accompanied by more negative nuclear attraction energies. Coulombic interactions with the electrons and nuclei of the borohydride ligand are larger, but almost no force is exerted on Ca in the z direction for this nonbonding FDA.

The most diffuse Ca s orbitals are the largest contributors to the FDA of $\tilde{D}^2A_1$. Note the nodal contours in Figure 4. Near Ca, one has an sp hybrid with an internal and an external node. Another nodal contour surrounds the B nucleus and the terminal H. This FDA is primarily a diffuse sp hybrid that has been orthogonalized to orbitals describing the terminal B–H bond. All of the properties of the FDA in Table IX are compatible with the idea of a diffuse electron, polarized to the right, with reduced nuclear contacts.

Examination of the FDA for $\tilde{E}^2E$ in terms of basis orbitals shows a predominance of the two most diffuse Ca p orbitals, with smaller mixtures of the tightest Ca d orbitals. Figure 5 shows this FDA. It must be remembered that this plot shows the FDA in the vicinity of the nuclei. A nodal contour in the region between Ca and B indicates an antibonding relationship. Ca d orbitals are assisting diffuse p orbitals in establishing this relationship. Note how the nodal contours that lie between the d orbital lobes to the right of Ca are turning back on themselves. This indicates that most of the space above the z axis and to the right of B has positive values of the FDA. (Plots on a larger scale confirm this.) There is a relatively large difference between the diagonal and nondiagonal second-order electron affinities for this state. Nondiagonal FDA's have lower $\langle z \rangle$ values and more negative

Table IX. Expectation Values of FDA's (au)

property	$\tilde{D}^2A_1$	$\tilde{E}^2E$	$\tilde{F}^2A_1$	$\tilde{G}^2E$	$\tilde{H}^2E$
kinetic property	0.158	0.765	0.246	0.176	0.212
total nuclear attraction energy	−3.335	−7.474	−3.827	−3.481	−3.455
$\langle z \rangle$	6.822	1.585	2.223	5.707	1.626
$\langle x^2 + y^2 \rangle$	71.958	62.135	90.154	103.709	150.648
Ca nuclear attraction energy	−2.567	−6.012	−2.935	−2.531	−2.651
B nuclear attraction energy	−0.425	−0.837	−0.497	−0.540	−0.447
H_t nuclear attraction energy	−0.075	−0.124	−0.089	−0.087	−0.079
H_b nuclear attraction energy	−0.089	−0.177	−0.102	−0.102	−0.093
E_z at Ca	0.012	−0.001	−0.002	0.001	0.000
E_z at B	0.006	0.017	0.006	0.006	0.005
E_z at H_t	0.005	0.016	0.004	0.008	0.004
E_z at H_b	0.006	0.009	0.005	0.005	0.005
E_y at H_b	−0.001	−0.014	−0.003	−0.005	−0.001

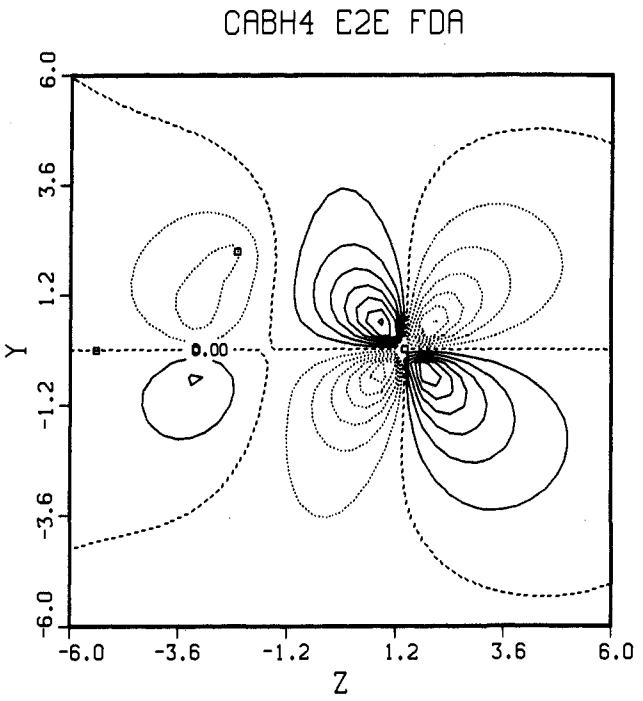

Figure 5. $\tilde{E}^2$E Feynman–Dyson amplitude of C_{3v} $CaBH_4$.

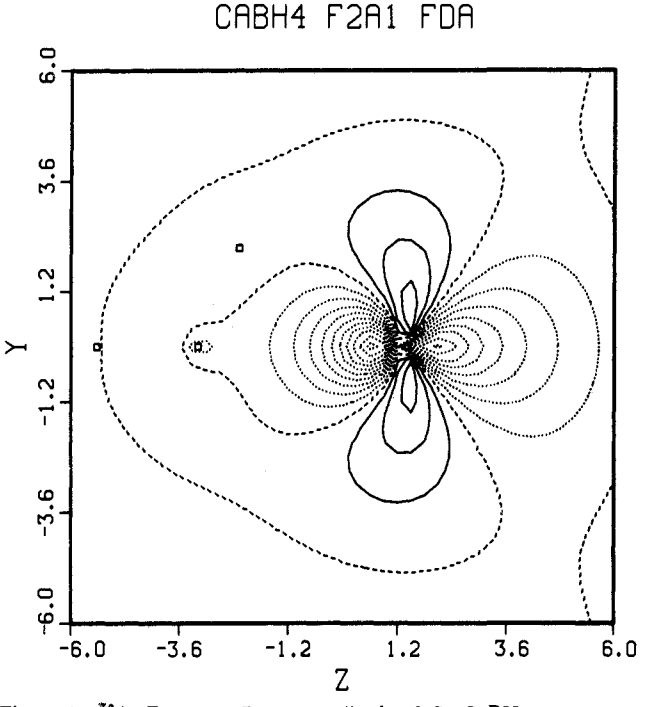

Figure 6. $\tilde{F}^2A_1$ Feynman–Dyson amplitude of C_{3v} $CaBH_4$.

nuclear attraction energies than their diagonal counterparts.

Extensive mixing of the diffusest s and p Ca orbitals with the second most diffuse Ca d orbital characterizes the FDA of $\tilde{F}^2A_1$. Because the tightest orbital of any consequence is a Ca d, one sees primarily d character in the vicinity of the nuclei (Figure 6). Nodal surfaces surround the bonding regions and there is another node far to the right of Ca. Along the z axis, the FDA is positive on the right extreme and negative on the left extreme. Examination of Table IX shows a large value of $\langle x^2 + y^2 \rangle$ and small nuclear attraction energies. These results are compatible with the notion of this FDA as a very diffuse sp hybrid polarized away from the ligand.

Diffuse d orbitals on Ca are the primary components of the FDA of $\tilde{G}^2$E. Interference with diffuse Ca p orbitals and the middle p orbitals on B produce the pattern of Figure 7, where a d–p hybrid has an antibonding relationship with B p orbitals. This

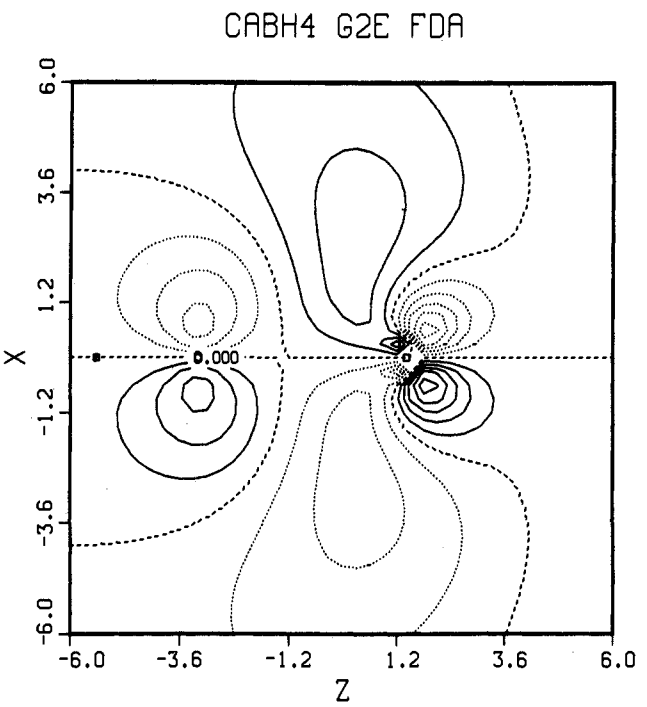

Figure 7. $\tilde{G}^2$E Feynman–Dyson amplitude of C_{3v} $CaBH_4$.

yields the large value for $\langle z \rangle$, for much of the electron density is pushed to the right.

The last state whose energy and FDA are stable with respect to basis set improvements is $\tilde{H}^2$E, which strongly resembles $\tilde{C}^2$E in its angular properties. In the FDA, which is composed almost exclusively of Ca d orbitals with Ca–B δ pseudosymmetry, the main contrast with $\tilde{C}^2$E is radical extent, a crude measure of which is given by $\langle x^2 + y^2 \rangle$.

4. C_{2v} Feynman–Dyson Amplitudes. In general, the FDA's of the C_{2v} form bear a strong resemblance to their C_{3v} counterparts, as suggested by the groupings in Table V. One of the 3-fold degenerate highest occupied molecular orbitals of the borohydride anion is composed of a B p_y orbital and an antisymmetric combination of s orbitals on the two terminal hydrogens. This orbital, with b_1 symmetry, has a smaller interaction with Ca than its perpendicular partner with b_2 symmetry. Splittings of ^{2}E states with π pseudosymmetry FDA's into $^2B_1$ and $^2B_2$ states place the former below the latter. In FDA's where the Ca–borohydride interaction is weak, the splittings are small. For the states correlating to the C_{3v} structure's $\tilde{E}^2$E state, however, the splitting is large, due to the pronounced antibonding interaction depicted in Figure 5. The vertical node between the ligand and Ca occurs at much lower z for $\tilde{F}^2B_1$'s FDA than for $\tilde{H}^2B_2$'s FDA. Energy separations between $\tilde{D}^2A_1$ and $\tilde{E}^2A_2$ or between $\tilde{L}^2A_1$ and $\tilde{M}^2A_2$ are small because of the δ pseudosymmetry of the FDA's. These trends are similar to those obtained for $CaNH_2$[4], another C_{2v} molecule in which the anionic ligand approaches Ca with filled a_1 and b_2 frontier orbitals.

IV. Discussion

Comparisons with molecules in which the borohydride ligand is replaced with methide, amide, hydroxide, fluoride, or hydrosulfide ligands reveal a similar splitting pattern for the lowest states.[4,5] In all cases, the ground state has an FDA dominated by Ca s orbitals that are polarized away from the ligand by Ca p orbitals. The next state (or pair of states, depending on whether there is a 3-fold axis of symmetry) has π pseudosymmetry with respect to the axis defined by Ca and the other non-hydrogen nucleus. Ca d and p orbitals contribute to these FDA's in proportions varying with the ligand. In general, the p contributions, as measured by coefficients of atomic orbitals in the FDA, are larger than d contributions. Ca p and d orbitals also mix in the following state, which exhibits σ pseudosymmetry, but the d orbitals tend to be more prominent than the p orbitals. All of

the lowest states are polarized away from the ligand. For every ligand studied so far, the next states have nonbonding FDA's with δ pseudosymmetry and are essentially defined by combinations of Ca d orbitals. For higher energies, the order of the states with respect to symmetry labels and pseudosymmetry classifications may vary, but there are still some common features. For $CaCH_3$ and $CaBH_4$, the next state's FDA consists chiefly of diffuse Ca s orbitals, polarized away from the ligand by the most diffuse Ca p orbitals. The nodal structure of this FDA ensures low overlap with the FDA for the ground state. (FDA's from approximate, nondiagonal calculations are not, in general, orthogonal to each other, although for the present cases, the overlaps are quite small.) There follows a π pseudosymmetry case displaying an antibonding relationship between Ca and ligand, but with the Ca hybrid polarized toward the ligand. For the borohydride-containing molecule, there is a favoring of p over d orbital contributions, while the opposite kind of mixture occurs for the methyl case. The next two states for $CaCH_3$ have FDA's with σ and π pseudosymmetry and exhibit a tendency to polarize toward the ligand. Two states for $CaBH_4$, $\tilde{F}^2A_1$ and $\tilde{G}^2E$, resemble these two from $CaCH_3$ in their nodal properties. For both molecules, the highest states whose energies are stable with respect to basis set improvements have FDA's with δ pseudosymmetry.

A recent communication of experimental work[19] holds that the lowest excited state and the next excited state have a reversed order from the ordering of Table V. Vibrational spacings in this report are in close agreement with the lowest frequency of Table II. While the excitation energy for $\tilde{A}^2E$ of 1.887 eV is just 0.02 eV below the peak assigned to the (0,0) transition, for the $\tilde{B}^2A_1$ calculated excitation energy of 2.039 eV, there is a discrepancy of 0.2 eV. The overestimate obtained with the present methods for the $CaCH_3$ $\tilde{B}^2A_1$ excitation energy is 0.08 eV. For the $\tilde{A}^2E$ $CaCH_3$ state, calculations underestimate the excitation energy by 0.11 eV. If these two correction factors are applied to the data of Table V, one obtains the opposite ordering of the two states, but they are within 0.04 eV of each other. Given this small energy difference and the flatness of the potential energy surface implied by the lowest two frequencies of Table II, one has propitious conditions for vibronic coupling. Extensive explorations of the excited state potential energy surfaces, especially in geometries with no 3-fold axis of symmetry, will be needed to clarify the order of the first two excited states. Although such an effort is beyond the scope of this investigation, it is worth remarking that the borohydride ligand has a tendency to enter into fluxional geometric relations with divalent metals, such as Be.[20] $Be(BH_4)_2$ has two stable minima with doubly bridged and triply bridged minima that lie within 1 kcal/mol of each other, according to recent investigations.[4,5] The present $CaBH_4$ results contrast with the larger separations of states obtained with other ligands. These other ligand deploy a lone pair of electrons in a σ relationship to the metal and, except for the $CaCH_3$ case, there are also occupied π frontier orbitals on the ligand. Because the σ lone pair points directly at Ca, the σ d orbital is destabilized with respect to the π d orbitals. For $CaBH_4$, however, the frontier orbitals of the anion are a 3-fold degenerate set consisting of a σ and two π members. One can therefore anticipate a smaller splitting between these two states or even a reversal of their order. Comparison of the calculated excitation energies of $CaCH_3$ (1.714 and 2.068) with their counterparts in Table V shows an insignificant change in the $\tilde{B}^2A_1$ state, but there is a destabilization of 0.17 eV for $\tilde{A}^2E$. Unlike the other anions, borohydride's π frontier orbitals confront the metal atom through bridging hydrogens. This is likewise true for the σ interaction, but the consequence is to diminish rather than strengthen the destabilization of Ca d_{z^2} with respect to the other cases.

V. Conclusions

Electron propagator calculations generate ground- and excited-state energies of $CaBH_4$ in its equilibrium, C_{3v} geometry. Analysis of correlated FDA's provides a one-electron interpretation of how the states differ from each other. Although the splitting between the first two excited states is smaller than that obtained for CH_3, NH_2, OH, F, and SH ligands, there is a basic pattern in molecules comprised of Ca and a ligand with a positive electron affinity.[4,5] The lowest level FDA is primarily a nonbonding Ca s–p hybrid and the following five levels are formed from Ca d orbitals perturbed by the ligand environment. D orbitals with δ pseudosymmetry with respect to the ligand exhibit little delocalization or hybridization, but there is considerable hybridization with p orbitals in the other three states. For higher energy states, diffuse Ca orbitals dominate the FDA's. One can characterize the contour plots, properties, and expansions in terms of basis orbitals as belonging to diffuse orbitals that have been orthogonalized to the orbitals near the nuclei that describe chemical bonding and to Ca core orbitals. For this reason, one often sees nodal surfaces bending around the periphery of the nuclei or far to the side of Ca away from the ligand. The latter type of node pertains to atomic orbitals with high principal quantum numbers and many radial nodes. Some of these higher states possess considerable antibonding character between Ca and the ligand.

Acknowledgment. An allocation from the Pittsburgh Supercomputer Center made these calculations possible. Dr. P. F. Bernath of the University of Arizona supplied a preprint of his experimental paper. This material is based on work supported by the National Science Foundation under Grant No. CHE-8723185. The government has certain rights in this material.

(19) Pianalto, F. S.; Bopegedera, A. M. R. P.; Fernando, W. T. M. L.; Hailey, R.; O'Brien, L. C.; Brazier, C. R.; Keller, P. C.; Bernath, P. F. *J. Am. Chem. Soc.* **1990**, *112*, 7900.

(20) Stanton, J. F.; Lipscomb, W. N.; Bartlett, R. J. *J. Chem. Phys.* **1988**, *88*, 5726. Ortiz, J. V.; Lipscomb, W. N. *Am. Inst. Phys. Proc.* **1986**, *140*, Emin, D., Aselage, T., Beckel, C. L., Howard, I. A., Wood, C., Eds., American Institute of Physics: New York.